Research article

Abdoulaye Ndao, Liyi Hsu, Wei Cai, Jeongho Ha, Junhee Park, Rushin Contractor, Yuhwa Lo and Boubacar Kanté*

Differentiating and quantifying exosome secretion from a single cell using quasi-bound states in the continuum

https://doi.org/10.1515/nanoph-2020-0008
Received January 5, 2020; revised February 19, 2020; accepted March 12, 2020

Abstract: One of the key challenges in biology is to understand how individual cells process information and respond to perturbations. However, most of the existing single-cell analysis methods can only provide a glimpse of cell properties at specific time points and are unable to provide cell secretion and protein analysis at single-cell resolution. To address the limits of existing methods and to accelerate discoveries from single-cell studies, we propose and experimentally demonstrate a new sensor based on bound states in the continuum to quantify exosome secretion from a single cell. Our optical sensors demonstrate high-sensitivity refractive index detection. Because of the strong overlap between the medium supporting the mode and the analytes, such an optical cavity has a figure of merit of 677 and sensitivity of 440 nm/RIU. Such results facilitate technological progress for highly conducive optical sensors for different biomedical applications.

***Corresponding author: Boubacar Kanté,** Department of Electrical Engineering and Computer Sciences, University of California, Berkeley, CA 94720, USA; and Department of Electrical and Computer Engineering, University of California San Diego, La Jolla, CA 92093-0407, USA, e-mail: bkante@berkeley.edu. https://orcid.org/0000-0001-5633-4163
Abdoulaye Ndao, Liyi Hsu, Jeongho Ha and Junhee Park: Department of Electrical Engineering and Computer Sciences, University of California, Berkeley, CA 94720, USA; and Department of Electrical and Computer Engineering, University of California San Diego, La Jolla, CA 92093-0407, USA
Wei Cai and Yuhwa Lo: Department of Electrical and Computer Engineering, University of California San Diego, La Jolla, CA 92093-0407, USA
Rushin Contractor: Department of Electrical Engineering and Computer Sciences, University of California, Berkeley, CA 94720, USA

Keywords: bound states in continuum; sensing; exosomes.

1 Introduction

Optical sensors have seen considerable growth as a result of an increasing number of applications in several domains such as health, defense, security, automotive, aeronautics, and quality control, to name a few [1–13]. Recent advances made in photonics, both in understanding physical phenomena and in the control of fabrication processes, have contributed to improved detection capabilities in terms of high stability and miniaturization of interfaces or system integration.

However, quantifying single-cell secretion using high-quality (high-Q) factor optical sensors is yet to be done. The analysis of individual cell secretion is essential to fully understand the functional heterogeneity and decipher the underlying mechanisms of cellular interactions and communication. Intercellular signaling and formation of cellular networks is a highly dynamic process mediated by the expression and secretion of small proteins (e.g. cytokines) and other molecules that govern particular cell activities, behaviors, and functions. The sensitive monitoring and analysis of cell secretion provide invaluable information on the specific functionality and real-time activity of individual cells in physiological or pathological processes. However, such dynamic and accurate analysis is still an unresolved challenge. The past few years have seen the advances in innovative strategies for both cell isolation and protein secretion analysis to enable single-cell resolution [1], for example, a large-scale micro-engraved array that is able to generate the populational secretion profiles from a single cell [2, 3]. Immunofluorescence staining is also widely used for protein studies, yet the necessity of intensive washing steps dramatically impairs the temporal resolution of the analysis [4]. Droplet microfluidics has been presented as a promising platform for single-cell

sorting and analysis [5]. However, subsequent secretion quantification requires external readout means, such as flow cytometry or spectroscopic methods, that increase the overall system complexity and only provide an endpoint result. To overcome these limitations, we proposed to use bound states in the continuum (BICs) [14–17] to identify and quantify single-cell secretion.

Cavities with high-Q values are in strong demand in nano-optics because of a large number of applications requiring strong light-matter interaction, such as biosensors, compact spectral-splitting solar cells, low-threshold lasers, and single-photon sources. However, "pure" BICs found in symmetric structures have a theoretically infinite Q factor, which renders the electromagnetic mode invisible in the reflection or transmission spectrum. Hence, asymmetric structures [18–28] have been proposed to achieve finitely high-Q factors for ultracompact optical sensors. Moreover, quantifying exosome secretion from a single cell using optical sensors requires not only high-Q but also a strong overlap between the mode of the cavity and the analyte (exosomes) in the entire system, as well as surface compatibility with the medium supporting the resonant mode and exosome functionalization. Therefore, developing an optical sensor with such field profile allows large interaction volumes between analytes and optical fields, which is fundamental for many applications, particularly biosensing. Hence, we propose and experimentally demonstrate a simple method to quantify in vitro single-cell secretion using an asymmetric all-dielectric nanostructure.

To experimentally quantify the exosomes, we use quasi-BICs, giving rise to a high figure of merit (FOM) of 667. Our system consists of an asymmetric, all-dielectric nanostructure composed of two silicon bars with slightly different widths on top of a silicon dioxide substrate. The system is illustrated in Figure 1, and exosomes are shown bonding on top of the optical sensor.

We performed numerical simulations (reflectance and field distributions) presented in Figure 2 to evaluate the optical responses of the designed asymmetric nanostructure. The structure is illuminated at normal incidence with polarization along the long axis of the dielectric bars (x polarization). Figure 2A presents the geometry of the unit cell. The incident wave is transverse magnetic (TM) polarized light (H field is along the y-axis). The substrate is silicon dioxide (SiO_2) with refractive index 1.46, and the two bars are silicon with refractive index 3.45. The period (p) of the array is 810 nm. The length (L) of the silicon bars is 600 nm, the thickness (h) of the bars is 320 nm, and the widths of the top bars are 230 nm (w_1) and 190 nm (w_2). The gap (g) between two bars is 125 nm. The thickness of the cladding layer (h_c) is 340 nm, which is 20 nm thicker than the silicon bars. High-Q factor appears around 1550 nm because of the asymmetry of the structure. The justification for using an asymmetric design is provided in Figure 2B, which shows the reflectance spectrum with respect to asymmetry of the nanostructure at normal incidence. When the asymmetry parameter $\Delta w/w_1$ is 0, the resonance turns into a perfect BIC and disappears from the spectrum. As the asymmetry of the structure increases, the bound state turns into a leaky resonance with increasing width. A finite linewidth is necessary to probe the perturbation induced by the analyte; therefore we choose w_2 to be 190 nm. Figure 2C shows the reflectance spectrum for the chosen design and Figure 2D shows the simulated electric and magnetic field distributions at the resonance. The magnetic field is confined between the two bars (low refractive index) while the electric field is confined at the edge of the bars. Such strong confinement enhances the sensing capability of the optical sensors and reduces drastically the quantity of the analyte to be sensed. Figure 2E represents the simulated reflection for different cladding layers ($n=1$ and $n=1.1$), while Figure 2F

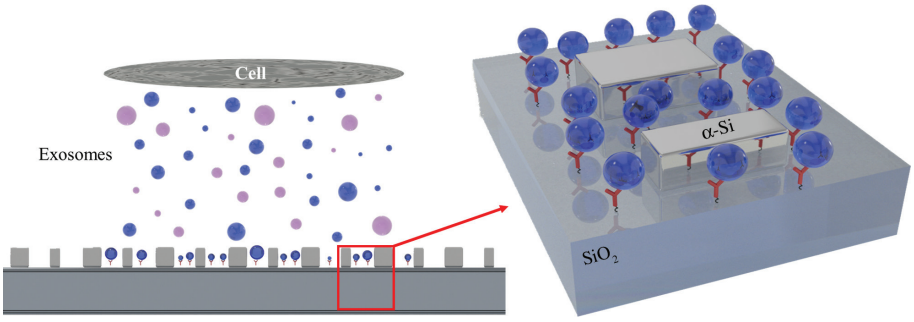

Figure 1: Design of the quasi-BIC supporting a high-Q mode.
Schematic of functionalized all-dielectric nanostructure showing the collection of exosomes secreted by a single cell.

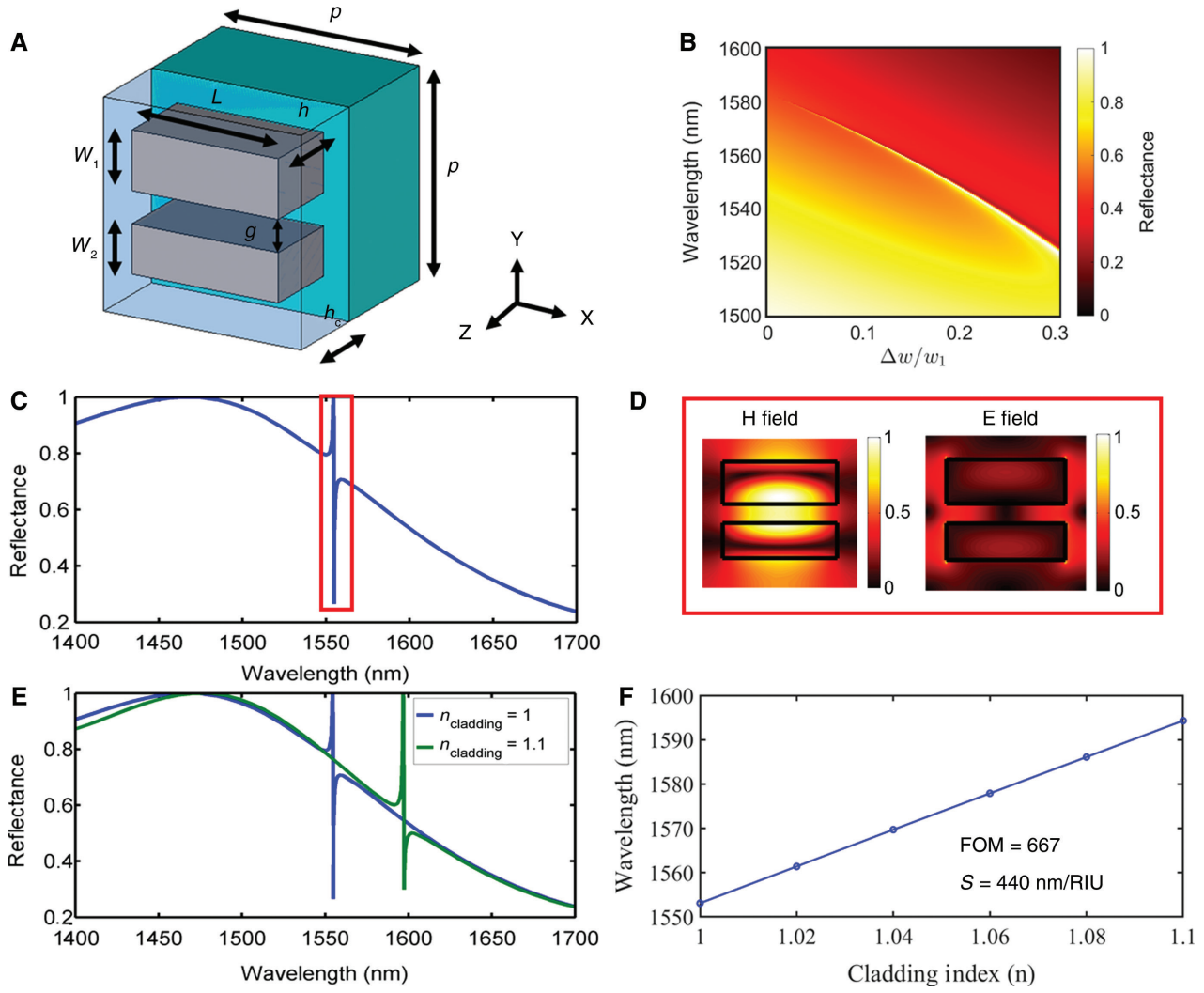

Figure 2: Numerical simulation of the quasi-BIC structure.
(A) Geometry of unit cell. (B) Reflectance spectrum with respect to the asymmetry of the nanostructure at normal incidence. (C) Reflectance through the nanostructure illustrating the resonance of the mode. To have the high-*Q* mode at 1550 nm, we choose the appropriate geometrical parameters. (D) Simulated electric and magnetic field distributions, in which the magnetic field is strongly localized between the two bars (low refractive index) while the electric field is highly confined in the edge of the bars. (E) Simulated reflection for different cladding layers ($n=1$ and $n=1.1$). (F) Resonance wavelength as a function of the refractive index of the surrounding medium, showing a high FOM of 677 and bulk sensitivity of 440 nm/RIU.

demonstrates the resonance shifts as a function of the fractive index of the surrounding medium.

To evaluate the sensing capability of our optical devices, we calculate both the spectral shift known as bulk refractive index sensitivity, which is defined as the ratio of the resonant wavelength shift $\Delta\lambda_R$ to the variation of the surrounding refractive index Δn (RIU).

FOM is defined as the ratio of the bulk refractive index sensitivity (S) to the full width at half-maximum (FWHM) of corresponding resonance:

$$S=\frac{\Delta\lambda_R}{\Delta n}[nm/\mathrm{RIU}], \tag{1}$$

$$FOM=\frac{S}{FWHM}. \tag{2}$$

On the basis of the above definitions, we calculated the bulk refractive index sensitivity (S) and the FOM, which are, respectively, 440 nm/RIU and 667. By combining the high-*Q* factor and strong field confinement in the air gap, our device meets the requirements of highly sensitive optical sensors.

The structure is fabricated using electron beam lithography (Vistec EBPG5200) on a silicon thin film, followed by dry reactive ion etching to form the quasi-BIC sensors. Figure 3 presents the top view of the SEM images, which

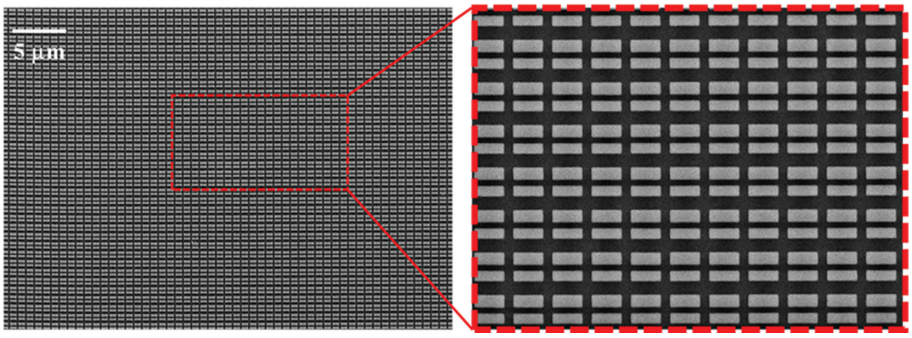

Figure 3: SEM image of the fabricated quasi-BIC.
Top-view SEM images of the nanostructure (left) and zoom (right), clearly evidencing the asymmetry of the nanostructure in order to excite the Fano mode. The SEM images show the successful fabrication of our device with good quality.

show the successful fabrication of our device with good quality.

To quantify the robustness of the sensor to the incidence angle, we performed numerical simulations and calculated the reflection at different angles. Experiments were performed using a customized setup composed of two main systems for illumination and detection for different angles [17, 28]. First, the sample is illuminated by a supercontinuum white light source after it is collimated, polarized along the length of the bar, and focused onto the sample using a parabolic mirror. The detection part consists of a multimode fiber on top of a rotation stage to collect the reflected light from the sample to an optical spectrum analyzer (OSA; APEX Technologies). To accurately measure the reflection for different angles, both the sample and the fiber for collection are mounted on the rotation stage with a resolution of 0.5°. For normal incidence, we used a lens with a very small numerical aperture (NA = 0.0025) to illuminate our device.

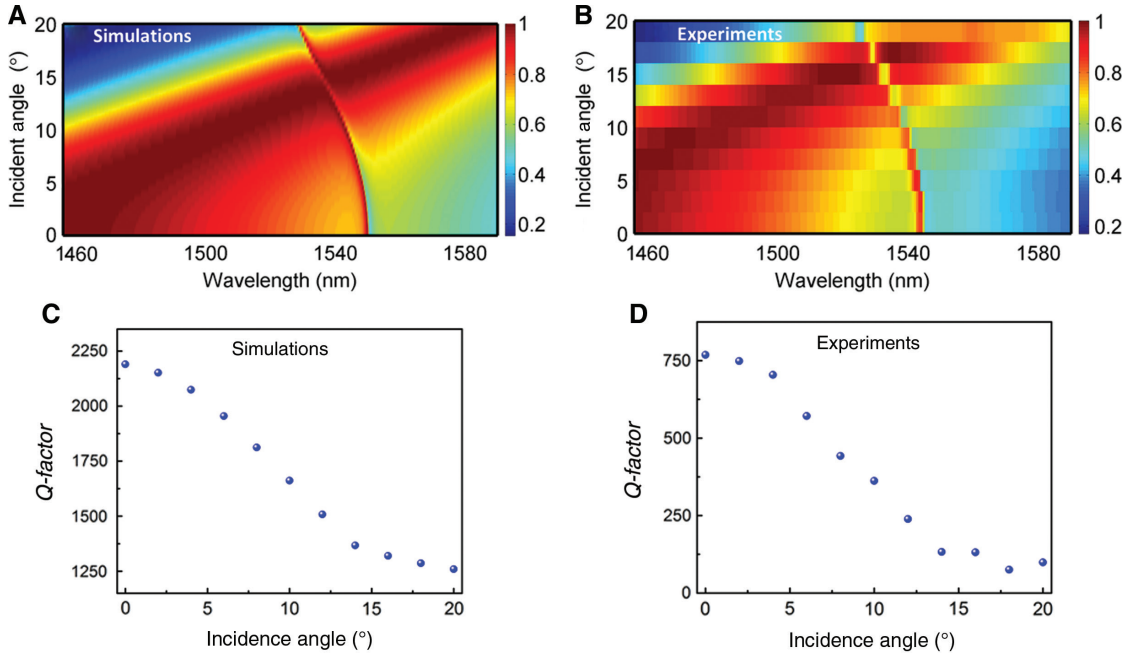

Figure 4: Angular response of the quasi-BIC structure.
(A) Numerical simulations of the reflectivity for different incidence angles using CST from 0° to 20°. (B) Measured reflectivity for different incidence angles from 0° to 20°. (D) Extracted quality factor from the experimental results as a function of the incidence angle. (C) Quality factor obtained by rational fitting as a function of the incidence angle, evidencing that the sensor has higher *Q* factor at normal incidence. (C) and (D) show good agreement between experiment and numerical simulations. The discrepancy between the quality factor from simulations (2×10^3 at normal incidence) and that from the experiment (750 at normal incidence) is due to the finite size and fabrication imperfections (mostly the roughness of the silicon substrate).

Figure 4A, B shows a good agreement between numerical simulations and experimental results. Figure 4C, D shows that *Q* factor decays as a function of the incidence angle, which confirms that our device can be a good candidate for optical microfluidic platforms.

After successfully fabricating and measuring our optical device, the next step consists of functionalizing the device with a view to quantifying exosomes from a single cell. To functionalize the device (Figure 5A), we first immobilize anti-CD9/anti-CD81 on SiO_2 by a standard protein immobilization protocol [29, 30]. Then the device (full area of the sample) was immersed in MCF7 condition culture medium for exosome binding. After binding, the device was cleaned and air-dried by blowing N_2. After this step, the device is ready for measurements.

To estimate the exosome number in the MCF7 condition culture medium (Figure 5B), we immobilized anti-CD63 on a cover glass with the protocol described above, and then immersed the cover glass in MCF7 condition culture medium. After the exosomes were collected on the functionalized cover slide, they were bound with the secondary antibody and Q-dots.

The cover slide was subsequently incubated in a solution of 10 nM streptavidin-coated Q-dots (Life Technologies) at room temperature for 1 h, followed by washing three times at 50°C in TBST and two times at 50°C in deionized (DI) water before drying by a series immersion steps of the slide in dilute ethanol with DI water. The sample was then imaged using an inverted fluorescent microscope (BE-II 9000, Keyence) with excitation/emission filters of 405/10 nm and 536/40 nm, respectively. The fluorescent images were processed through haze reduction and black balance algorithms, and the Q-dots were counted using an object counter module in the microscope software (BZ-II Analyzer). The measurement results clearly show that the exosome secreted by MCF7 has more CD9 than CD81 (see Figure 6A). Similarly, we evaluated the sensing ability of our system by measuring the resonance shift of our device for different concentrations of exosomes. Figure 6B clearly shows that, for different

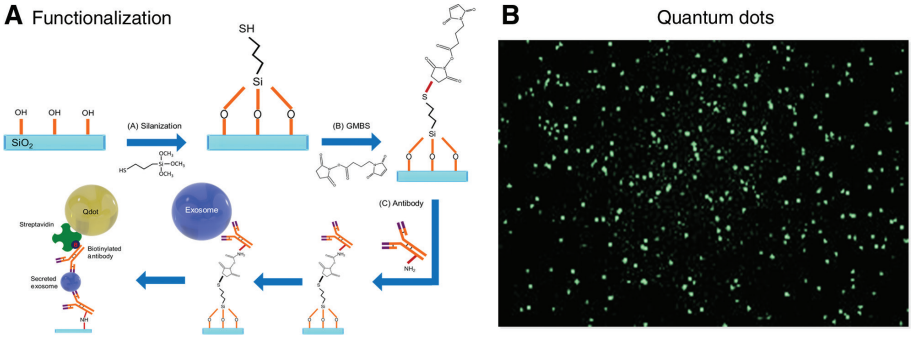

Figure 5: Functionalization and quantification of exosomes using quantum dots.
(A) Flowchart to functionalize the optical sensors in order to quantify exosome secretions. (B) Fluorescent images were processed through haze reduction and black balance algorithms, and Q-dots (number of quantum dots) were counted using the object counter module in the microscope software (BZ-II Analyzer).

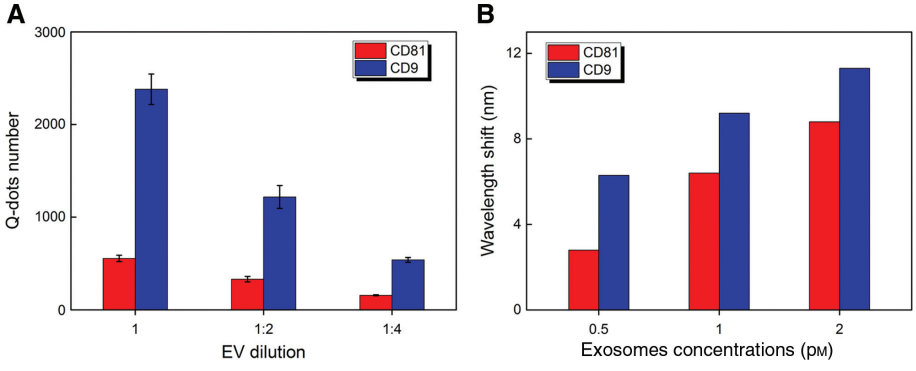

Figure 6: Identification and quantification of exosomes using the quasi-BIC structure.
(A) Number of Q-dots (counted by the object counter module in the microscope software) as a function of the EV dilution. (B) Exosome concentration for both CD81 and CD9 as a function of the wavelength shift, evidencing that the quantity of CD9 is higher than that of CD81 for the cell.

concentrations, the resonance shift corresponding to CD9 is always higher than that corresponding to CD81, which demonstrates that our optical sensor can detect the difference at very low concentrations.

2 Conclusion

In conclusion, we have designed and experimentally demonstrated a new type of optical sensor to quantify not only the exosomes but also the surface protein on the exosome. Our optical sensors demonstrated refractive index detection with high sensitivity. Because of the strong overlap between the medium supporting the mode and the analytes, such an optical cavity has an FOM of 677 and sensitivity of 440 nm/RIU. Our optical sensors meet all the requirements for exosome detection such as high-Q factor, strong overlap between the mode and the exosomes, and a functionalizable surface, which is not the case for many optical sensors with high-Q values. Our results facilitate technological progress for highly conducive optical sensors for different biomedical applications.

References

[1] Yu J, Zhou J, Sutherland A, Wei W, et al. Microfluidics-based single-cell functional proteomics for fundamental and applied biomedical applications. Annu Rev Anal Chem 2014;7:275–95.
[2] Love JC, Ronan JL, Grotenbreg GM, Van Der Veen AG, Ploegh HL. A microengraving method for rapid selection of single cells producing antigen-specific antibodies. Nat Biotechnol 2006;24:703–7.
[3] Torres AJ, Hill AS, Love JC. Nanowell-based immunoassays for measuring single-cell secretion: characterization of transport and surface binding. Anal Chem 2014;86:11562–9.
[4] He M, Crow J, Roth M, Zeng Y, Godwin AK. Integrated immunoisolation and protein analysis of circulating exosomes using microfluidic technology. Lab on a chip. 2014;14:3773.
[5] Wen N, Zhao Z, Fan B, et al. Development of droplet microfluidics enabling high-throughput single-cell analysis. Molecules 2016;21:1–13.
[6] Liu N, Weiss T, Mesch M, Langguth L, Eigenthaler U, Hirscher M. Planar metamaterial analogue of electromagnetically induced transparency for plasmonic sensing. Nano Lett 2010;10:1103–7.
[7] Wu C, Khanikaev AB, Adato R, et al. Fano-resonant asymmetric metamaterials for ultrasensitive spectroscopy and identification of molecular monolayers. Nat Mater 2012;11:69–75.
[8] Miroshnichenko AE, Kivshar YS. Fano resonances in all-dielectric oligomers. Nano Lett 2012;12:6459–63.
[9] Im H, Shao H, Park YI, et al. Label-free detection and molecular profiling of exosomes with a nano-plasmonic sensor. Nat Biotechnol 2014;32:490–5.
[10] Kuznetsov AI, Miroshnichenko AE, Brongersma ML, Kivshar YS, Luk'yanchuk B. Optically resonant dielectric nanostructures. Science 2016;354:846.
[11] Park J-H, Kodigala A, Ndao A, Kanté B. Hybridized metamaterial platform for nano-scale sensing. Opt Express 2017;25:15590.
[12] Oh SH, Altug H. Performance metrics and enabling technologies for nanoplasmonic biosensors. Nat Commun 2018;9:5263.
[13] Tittl A, Leitis A, Liu M, et al. Imaging-based molecular barcoding with pixelated dielectric metasurfaces. Science 2018;360:1105–9.
[14] Hsu C, Zhen B, Lee J, et al. Observation of trapped light within the radiation continuum. Nature 2013;499:188–91.
[15] Kodigala A, Lepetit T, Gu Q, Bahari B, Fainman Y, Kanté B. Lasing action from photonic bound states in continuum. Nature 2017;541:196–9.
[16] Lepetit T, Kanté B. Controlling multipolar radiation with symmetries for electromagnetic bound states in the continuum. Phys Rev B 2014;90:241103.
[17] Sadrieva ZF, Sinev IS, Koshelev KL, et al. Transition from optical bound states in the continuum to leaky resonances: role of substrate and roughness. ACS Photon 2017;4:723–7.
[18] Koshelev K, Lepeshov S, Liu M, Bogdanov A, Kivshar Y. Asymmetric metasurfaces with high-Q resonances governed by bound states in the continuum. Phys Rev Lett 2018;121:193903.
[19] Fedotov VA, Rose M, Prosvirnin SL, Papasimakis N, Zheludev NI. Sharp trapped-mode resonances in planar metamaterials with a broken structural symmetry. Phys Rev Lett 2007;99:147401.
[20] Zhang J, MacDonald KF, Zheludev NI. Near-infrared trapped mode magnetic resonance in an all-dielectric metamaterial. Opt Express 2013;21:26721–8.
[21] Yang Y, Kravchenko II, Briggs DP, Valentine J. All-dielectric metasurface analogue of electromagnetically induced transparency. Nat Commun 2014;5:5753.
[22] Wu C, Arju N, Kelp G, et al. Spectrally selective chiral silicon metasurfaces based on infrared Fano resonances. Nat Commun 2014;5:3892.
[23] Moritake Y, Kanamori Y, Hane K. Experimental demonstration of sharp Fano resonance in optical metamaterials composed of asymmetric double bars. Opt Lett 2014;39:4057–60.
[24] Moritake Y, Kanamori Y, Hane K. Demonstration of sharp multiple Fano resonances in optical metamaterials. Opt Express 2016;24:9332–9.
[25] Campione S, Liu S, Basilio LI, et al. Broken symmetry dielectric resonators for high quality factor Fano metasurfaces. ACS Photon 2016;3:2362–7.
[26] Tuz VR, Khardikov VV, Kupriianov AS, et al. High-quality trapped modes in all-dielectric metamaterials. Opt Express 2018;26:2905–16.
[27] Zhang Y, Liu W, Li Z, et al. High-quality-factor multiple Fano resonances for refractive index sensing. Opt Lett 2018;43:1842–5.
[28] Ndao A, Belkhir A, Salut R, Baida FI. Slanted annular aperture arrays as enhanced-transmission metamaterials: excitation of the plasmonic transverse electromagnetic guided mode. Appl Phys Lett 2013;103:211901.
[29] Cai W, Chiu YJ, Ramakrishnan V, Tsai Y, Chen C, Lo YH. A single-cell translocation and secretion assay (TransSeA). Lab Chip 2018;18:3154–62.
[30] Chiu YJ, Cai W, Shih YR, Lian I, Lo YH. A single-cell assay for time lapse studies of exosome secretion and cell behaviors. Small 2016;12:3658–66.